Article

Indirect Evaluation of the Electrocaloric Effect in PbZrTiO$_3$ (20/80)-Based Epitaxial Thin Film Structures

Georgia A. Boni * , **Lucian D. Filip** , **Cristian Radu, Cristina Chirila** , **Iuliana Pasuk** , **Mihaela Botea, Ioana Pintilie** and **Lucian Pintilie**

National Institute of Materials Physics, Atomistilor 405A, 077125 Magurele, Romania
* Correspondence: andra.boni@infim.ro

Abstract: Electrocaloric effect is the adiabatic temperature change in a dielectric material when an electric field is applied or removed, and it can be considered as an alternative refrigeration method. Materials with ferroelectric order exhibit large temperature variations in the vicinity of a phase transition, while antiferroelectrics and relaxors may exhibit a negative electrocaloric effect. In this study, the temperature variation in polarization was investigated for epitaxial ferroelectric thin film structures based on PbZrTiO$_3$ materials in simple or complex multilayered structures. We propose the intriguing possibility of a giant negative electrocaloric effect ($\Delta T = -3.7$ K at room temperature and $\Delta T = -5.5$ K at 370 K) in a simple epitaxial Pb(ZrTi)O$_3$ capacitor. Furthermore, it was shown that abnormal temperature variation in polarization is dependent on the non-FE component introduced in a multilayered structure. No significant variation in polarization with temperature was obtained for PZT/STON multilayered structures around room temperature. However, for PZT/BST or PZT/Nb$_2$O$_5$ multilayers, an abnormal temperature variation in polarization was revealed, which was similar to a simple PZT layer. The giant and negative ΔT values were attributed to internal fields and defects formed due to the large depolarization fields when the high polarization of the FE component was not fully compensated either by the electrodes or by the interface with an insulator layer. The presented results make Pb(ZrTi)O$_3$-based structures promising for cooling applications operating near room temperature.

Keywords: negative electrocaloric effect; epitaxial thin films; PZT; pyroelectric coefficient

1. Introduction

Solid-state refrigeration technology via electrocaloric effect (ECE) is welcomed in many fields, such as modern electronics, communications, medical and military, etc., in order to replace traditional refrigeration technology using Freon gas [1,2]. ECE is defined as the change in the isothermal entropy or adiabatic temperature of dielectric materials when the electric field is changed, and it may represent the solution of converting electrical energy into thermal energy [3–7].

The direct methods used to characterize ECE in different materials imply calorimetric methods to directly measure the entropy variation (ΔS) or temperature sensors to measure temperature variation (ΔT) [6,8,9].

The most common methods found in the literature focusing on the ECE are based on an indirect method, which is obtained from the Maxwell relations [8]:

$$\left(\frac{\partial S}{\partial E}\right)_{T,X} = \left(\frac{\partial P}{\partial T}\right)_{E,X} \tag{1}$$

where S represents the entropy, E represents the electric field, P is polarization, and T is the temperature. When the electric field E is changed from E_1 to E_2, the entropy variation can be deduced as:

$$\Delta S = \int_{E_1}^{E_2} \left(\frac{\partial P}{\partial T} \right)_{E,X} dE \qquad (2)$$

Considering $TdS = -C_e dT$, where C_e is the specific heat capacity, and ρ is the density:

$$\Delta T = - \int_{E_1}^{E_2} \frac{T}{\rho C_e} \left(\frac{\partial P}{\partial T} \right)_{E,X} dE \qquad (3)$$

ECE can be observed in any dielectric material when the applied electric field induces a change in electric polarization. However, the most significant results are obtained in ferroelectric (FE) or antiferroelectric (AFE) materials, especially in the vicinity of the phase transition [10–13].

Conventional ECE implies $\frac{\partial P}{\partial T} < 0$ and is usually obtained in paraelectric phases or FE phases when the electric field and polarization have the same direction.

Inverse or negative ECE is obtained when $\frac{\partial P}{\partial T} > 0$ and is usually obtained in AFE materials for electric fields in the range of AFE–FE transition [14–16]. Similarly, negative ECE could be obtained in the FE phase under different conditions: when the electric field is antiparallel with polarization and induces switching, the non-collinearity between the electric field and polarization, or a phase transition between different FE phases, multilayers, or defects, induces dipoles [17–22].

Pb(Zr,Ti)O$_3$ is a well-known FE order perovskite material. Different Zr/Ti ratios give different structural symmetries and FE properties such as dielectric constant, polarization, or phase transition temperature. For the EC field, the most studied compositions are of Zr between 80% and 100% for which PZT is at the phase boundary between AFE and FE or in the AFE phase, respectively [3,23,24]. For these compositions, high levels of adiabatic temperature changes have been obtained close to the phase transition temperature. Additionally, doping with La on the A-site position with AFE or relaxor behavior has been intensively investigated for the EC effect [16,25]. More recently, multilayer structures based on PZT have been studied for large adiabatic temperature changes around room temperature: PZT–CFO multilayers or multilayered structures based on different PZT compositions of PZT exhibit large negative EC around RT [16,26,27].

Our study is based on the indirect evaluation of ECE in epitaxial FE thin film PbZrTiO$_3$ (20/80) (PZT). The simple PZT thin film capacitors have high-quality structures, with epitaxial growth and smooth interfaces. Electrical characterization reveals a rectangular hysteresis loop with high polarization and low leakage currents, compared with the switching and displacement currents specific for FE and insulators. Temperature variation in the 200–400 K range induces a polarization increase, which determines a negative ECE. XRD measurements between room temperature (RT) and 100 °C have not revealed a structural change, which is expected for this temperature range since the phase transition is expected to be over 680 °C [28]. This abnormal temperature dependence of polarization is tested for different multilayer configurations. Additional layers of semiconducting Nb-dopped SrTiO$_3$ or insulators such as BaSrTiO$_3$ or Nb$_2$O$_5$ are also used. For the case of a resistive-like additional layer, the multilayer polarization does not change near RT, while for FE/insulator multilayers, polarization increases as the temperature rises. These results demonstrate that the inverse ECE could be strongly influenced by external circuit elements or by changes in the electrostatic conditions induced by the non-FE components.

2. Materials and Methods

The structures were grown on SrTiO$_3$ (001) (STO) substrates, each structure in a single process, through pulsed laser deposition (PLD) using a workstation from Surface GmbH and commercial targets acquired from Pi-KEM Ltd., Tamworth, UK. The system uses a KrF excimer laser with a wavelength of 248 nm, a repetition rate of 10 Hz, and a

maximum energy of 700 mJ. The specific conditions used for the growth of the $SrRuO_3$ bottom electrodes and PZT layers have been published elsewhere [29,30]. Additional layers of semiconductor or insulator were deposited at the same temperature and repetition rate with the PZT layer, at an oxygen pressure between 0.14 and 0.2 mbar, and a fluence around 2 J/cm^2. Platinum square electrodes with 0.01 mm^2 were deposited ex situ via sputtering through stencil masks for electrical characterization.

The samples were electrically characterized at different temperatures in a Lakeshore cryostation with micro-manipulated arms, and hysteresis loops (P–V) were recorded using a TF 2000 aixACCT Systems.

XRD measurements were performed using a Rigaku-SmartLab X-ray diffractometer (Rigaku Corporation, Tokyo, Japan) with a conventional Cu anode X-ray tube, powered at 40 kV and 40 mA. The symmetric XRD scans corrected for the single crystal surface miscut, 2θ ω scans, were performed with a Ge(220) monochromator in the incident beam and a HyPix detector in 0D mode, in the 2θ range 18–26° and 38–50°. The reciprocal space mapping (RSM) images were taken with a HyPix 3000 camera in 2D mode, around $\chi = 0$ (symmetric to the sample surface), within 2θ = 35–51°, and $\chi = \pm 15°$. The XRD measurements above room temperature were performed by using a DHS 1100 temperature chamber (Anton Paar GmbH, Graz, Austria), in a normal atmosphere, with a temperature ramp rate of 10 °C/min and 5 min stabilization time at each temperature. The XRD measurements were performed at 30, 50, 70, and 100 °C, in the scan range.

TEM investigations were performed on an analytical electron microscope JEM-ARM 200 F operated at 200 kV.

3. Results

In Figure 1, the polarization–voltage measurements are shown for the 1 kHz frequency and 5 V amplitude at different temperatures between 200 K and 370 K for a 200 nm thickness epitaxial PZT layer deposited on the SRO bottom electrode. Ferroelectricity was present for the entire temperature range, and all measurements showed the characteristic rectangular shapes of the hysteresis loops with a sharp transition at the coercive voltage and very low leakage currents at higher voltages. It can be observed that the polarization dependence, for non-switching voltage ranges, had an atypical dependence on temperature. The polarization values increased from 65 μC/cm^2 to 95 μC/cm^2 as the temperature increased. The results are shown in Figure 2a for different voltages. A normal behavior implies a slow polarization decrease with temperature or an almost constant value if the measurement interval is much lower than the transition temperature. This normal behavior was obtained, for example, in polycrystalline PZT 20/80 deposited through sol–gel on SRO/STO (see Figure S2), where polarization was almost constant in the 100–300 K range for all voltages. A polarization variation with temperature is associated with a pyroelectric effect, and the indirect pyroelectric coefficient is deduced as dP/dT and represented in Figure 2b. The indirect pyroelectric coefficient increased as the temperature rose, and it also depended on the applied voltage, as it is shown in Figure S1b. Near RT, a value of 0.00175 C/m^{2}K was obtained for voltages around 2 V, and then it decreased to 0.00135 C/m^{2}K for 4 V. Using Equation (3), the adiabatic temperature change ΔT can be obtained, considering the heat capacity $C_e = 330$ JK^{-1}kg^{-1} and density $\rho = 8.3$ gcm^{-3}. The results are shown in Figure 2c. Due to the abnormal increase in polarization values when the temperature increased, negative values were obtained for ΔT, representing a negative ECE. Giant values of $\Delta T = -1$ K and $\Delta T = -5.5$ K were obtained at 370 K for 1 V and 3 V, respectively. At RT, a maximum of $\Delta T = -3$ V was obtained. These are very high values for adiabatic temperature changes when compared with the values of $|\Delta T| > 10$ K obtained for relaxor ferroelectrics [7,31,32], antiferroelectrics [7,14,33] or multilayers [26]. Additionally, large ΔT are characteristic for temperatures close to the phase transition, therefore a much higher temperature for PZT-based materials.
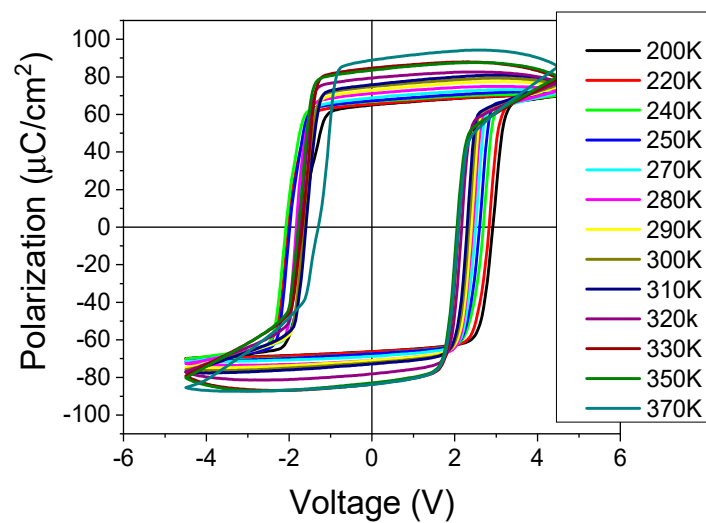
Figure 1. The hysteresis measurements performed between 200 K and 370 K at 1 kHz frequency and 5 V amplitude for epitaxial thin film PZT/SRO/STO.
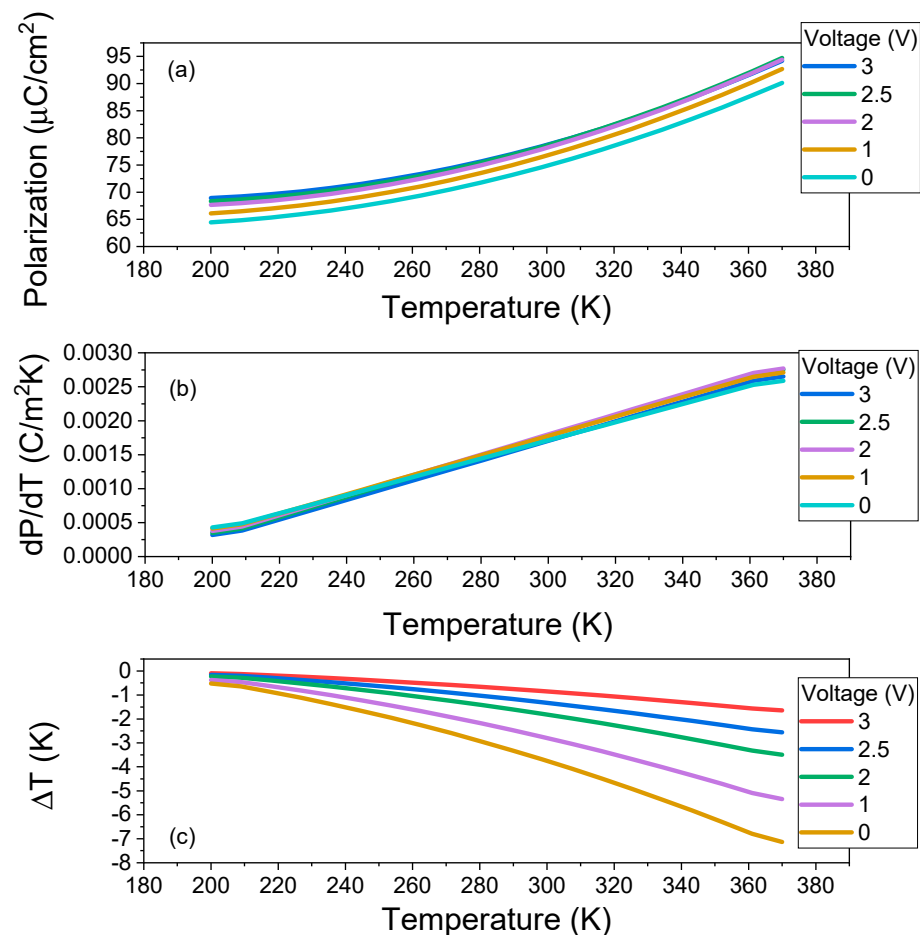

Figure 2. (**a**) The temperature dependence of polarization after switching for different voltages; (**b**) the indirectly evaluated pyroelectric coefficient as a function of temperature and different voltages; (**c**) the indirectly deduced adiabatic temperature variation as a function of temperature and voltages for epitaxial thin film PZT/SRO/STO.

One of the reasons why, sometimes, incorrect negative ECE is obtained from the indirect method (leading to a frequency and applied fields dependency [34,35]) is incomplete

switching (when a high frequency or a lower field is applied). Increasing the temperature, the coercive field decreased, and at the same maximum applied field, a complete switching could be obtained at elevated temperature, giving an apparent increase in polarization with temperature. In our case, at a lower temperature, the coercive voltage was 3.5 V, and the maximum applied voltage was 4.5 V. For good epitaxial thin films with a polarization perpendicular to the surface of the sample, switching was very fast. A variation from –P to +P was revealed in less than 1 V. For bulk ceramics or organic ferroelectrics, it is normal to perform PV measurements at lower frequencies, due to the large loading time/ large time constant systems. For epitaxial thin films such as the ones used in our study, at lower frequencies, the leakage current was much higher than the displacement current and resulted in many errors in the extraction of the remnant polarization.

The polarization increase with temperature is usually associated with larger conduction due to leakage currents. This measurement method is based on recording the total current and then integrating it over the time interval to deduce the polarization. However, in this case, the leakage current was much lower than the displacement current at this frequency. This was also corroborated by the results of the remnant hysteresis measurements, which were performed to exclude the non-switching contribution. In Figure S1a, the remnant hysteresis loops are represented for positive voltages at different temperatures, and it can be observed that polarization values were similar, while the polarization increase with increasing temperature is also presented. The epitaxial ferroelectric thin films, with high polarization as is the case of the PZT 20/80, could exhibit different domain configurations, due to the large depolarization fields induced during the deposition and cooling of the sample. The presence of a-type domains, with polarization oriented in-plane of the surface, is often reported. This domain did not contribute to the measured polarization along an axis perpendicular to the sample surface. A temperature increase could change the number of domains, and by decreasing their volumes, it may induce an extrinsic increase in polarization. For this purpose, the XRD measurements were performed for different temperatures between 30 °C and 100 °C and the results are shown in Figure 3.

The 2θ ω scans show only the 00 l lines of PZT, the pseudocubic SRO film, and the cubic STO substrate. As we commonly obtain for PZT/SRO/STO heterostructures, there are two kinds of PZT structures, a major one characterized by a smaller out-of-plane lattice constant and a minor component with a larger one. We interpret that the minor PZT component is a thin layer close to the interface, compressively strained due to the epitaxial accommodation to the smaller in-plane constant of SRO and STO [36]. We further named the stressed component PZT-s, in contrast to the other component, called relaxed PZT, PZT-r. The diffraction lines generated by the gold electrodes deposited on the heterostructure (for electrical measurements) are also visible. As shown in Figure 3a, the 2θ ω scans were performed around the 001 STO peak, where the layer oscillations of the SRO film are well visible, and around the 002 STO peak, where the better angular resolution allows us to follow the temperature-induced line displacements. It is observed that the SRO layer oscillations retained their clarity with temperature, showing that the smoothness of the SRO interfaces did not deteriorate with temperature in this range. The zoomed views presented at the bottom of Figure 3a emphasize the peak displacements caused by temperature. It is observed that the peak corresponding to PZT-r shifted toward larger angles, indicating a decrease in the c lattice parameter of the tetragonal PZT structure as the temperature increased. The PZT-s peak practically did not change and neither did the SRO and STO peaks in the investigated temperature range. The Au line shifted to lower angles, indicating the expected thermal expansion of the gold electrodes.
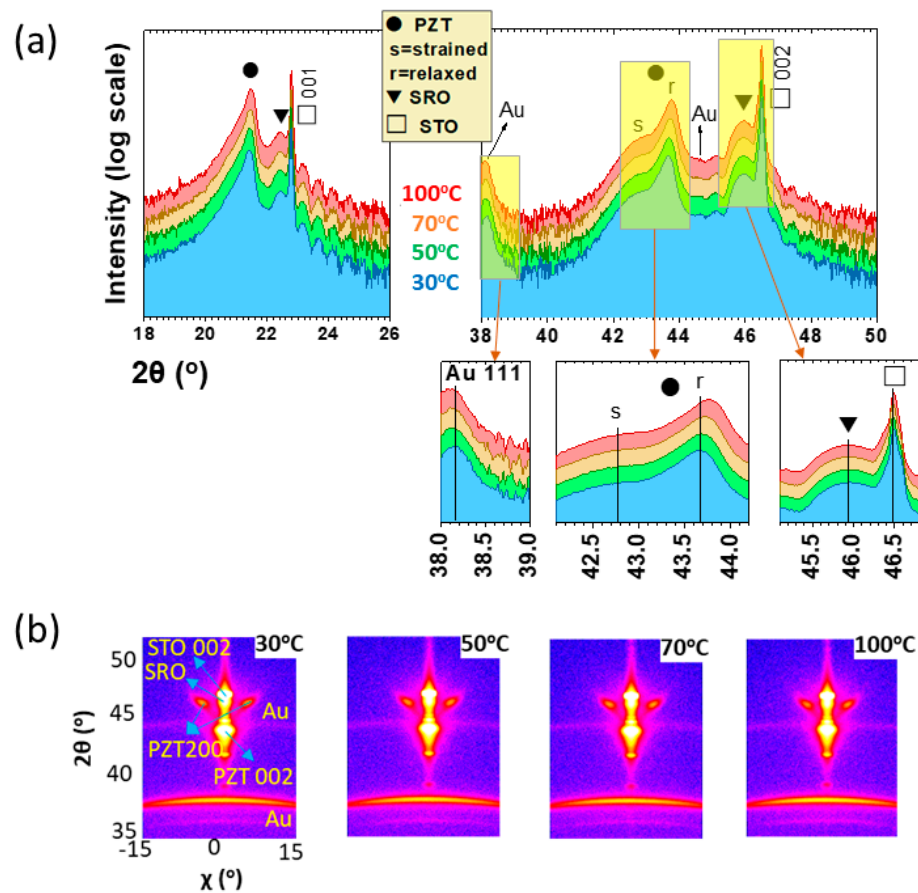
Figure 3. XRD measurements at different temperatures: (**a**) 2θ ω scan; (**b**) reciprocal space mapping around 002 STO.; the spots indicated as PZT 200 originate from tilted PZT-a domains [37].

It is known that epitaxial PZT thin films relax by alternating the majority of c-type domains with narrow a-type domains, which grow slightly tilted from the interface (at 2–3°), forming a typical c/a/c/a structure. Reciprocal space mapping (RSM) was performed in the vicinity of the 002 STO node at different temperatures in order to study the temperature dependence of the c/a/c/a structure. The diffraction spots recorded in (2θ, χ) coordinates were identified, as shown in Figure 2b. No noticeable changes were observed in the RSM images for this temperature range.

The evolution of polarization with temperature was further analyzed for multilayered structures based on epitaxial PZT 20/80 thin films. We analyzed the case of PZT in contact with a 10 nm thin layer of Nb-doped SrTiO3 (STON) in two different configurations: STON/PZT/SRO/STO or PZT/STON/SRO/STO. The STON thin film is known to be a semiconductor, and it is used to increase the non-FE external resistance. In Figure 4a,b, the hysteresis measurements at different temperatures are shown for the two configurations. Compared with the PZT thin film capacitor, a noticeable increase in the coercive voltage could be observed, due to increasing the total time constant of the circuit since the non-FE series resistance increased [38]. Polarization was almost constant at around 70–75 $\mu C/cm^2$ for the measured temperature range, and it showed no dependence on voltage.
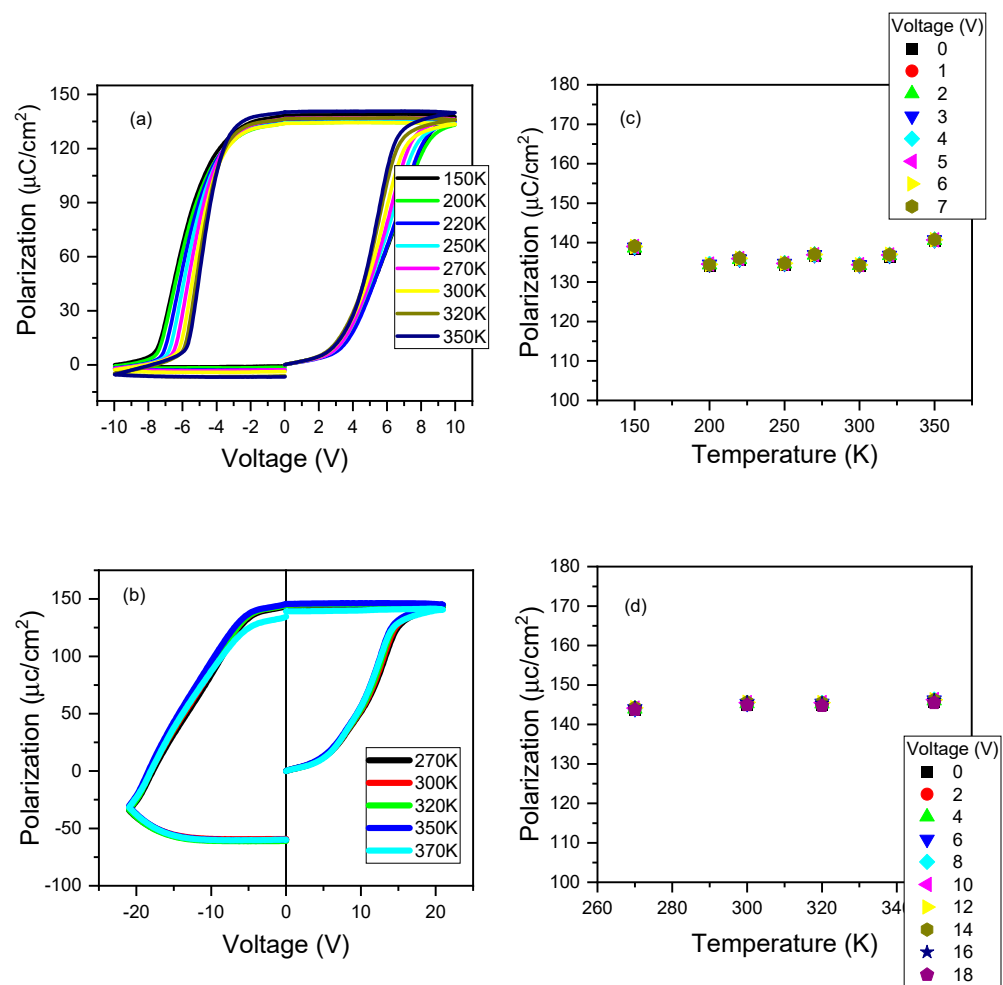
Figure 4. (**a**,**b**) The hysteresis measurements performed at different temperatures for STON/PZT/SRO and PZT/STON/SRO/STO; (**c**,**d**) the constant dependence of polarization as a function of temperature for STON/PZT/SRO and PZT/STON/SRO/STO.

Further multilayered structures were fabricated with two different insulator thin films deposited on top of the PZT layer: BST/PZT/SRO/STO and Nb_2O_5/PZT/SRO/STO. The presence of the insulator layer in contact with the main FE acted as a series capacitor. During switching, the series capacitor was charged and induced an internal field in the FE in the opposite direction to the polarization. This resulted in an induced back-switching effect at 0 V [38]. This phenomenon was revealed for both structures, as shown in Figure 5, for all temperatures. A reduction in the maximum polarization at RT to around 30 and 40 $\mu C/cm^2$ was obtained for Nb_2O_5/PZT/SRO/STO and BST/PZT/SRO/STO, respectively. This is explained by the high depolarization fields appearing in these multilayered structures during cooling after deposition at high temperatures. For these structures, the polarization increased with the increasing temperature, and it was found to have a similar behavior as the simple PZT layer, as can be observed in Figures 6a and 7a. The pyroelectric coefficient evaluated indirectly was reduced by a factor of ≈ 2 for both cases, compared with the simple PZT layer. A negative adiabatic temperature change was also obtained.
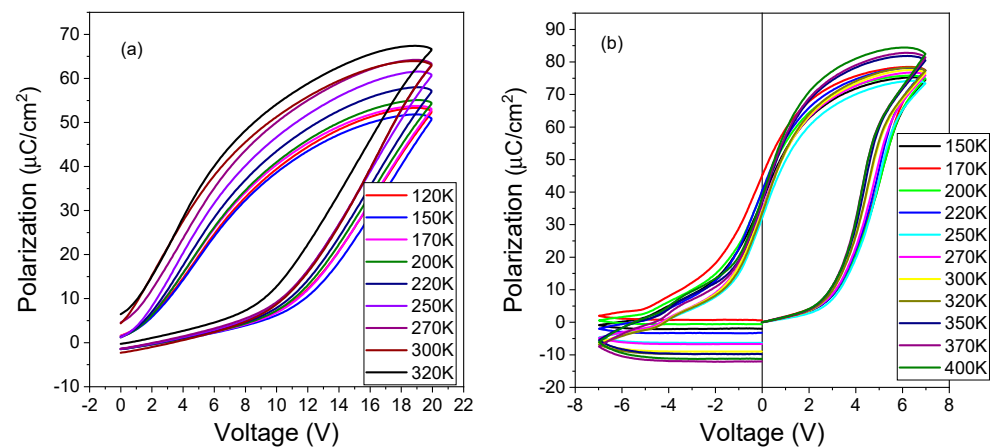
Figure 5. (**a**,**b**) The hysteresis measurements performed at different temperatures for Nb_2O_5/PZT/SRO and BST/PZT/SRO/STO.
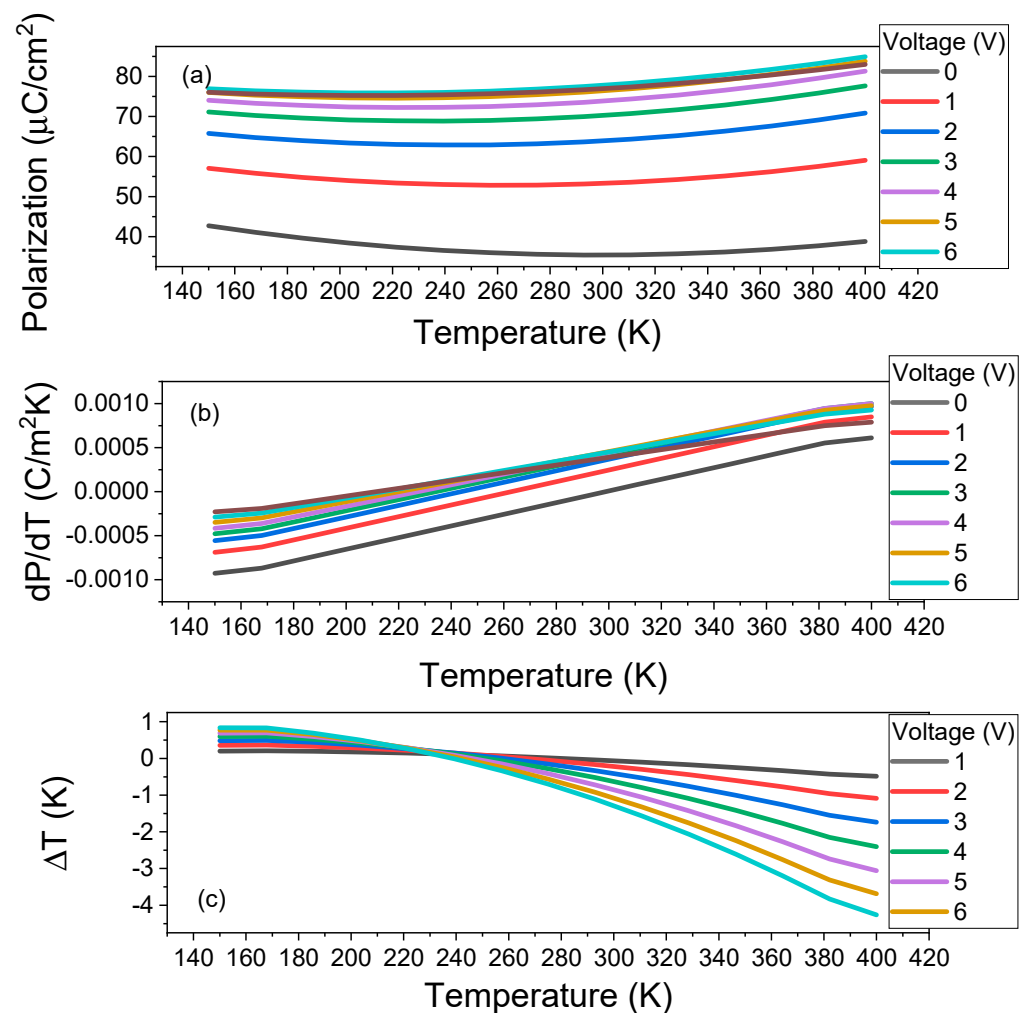

Figure 6. (**a**) The temperature dependence of polarization after switching for different voltages; (**b**) the indirectly evaluated pyroelectric coefficient as a function of temperature and different voltages; (**c**) the indirectly deduced adiabatic temperature variation as a function of temperature and voltages for epitaxial thin film BST/PZT/SRO/STO.
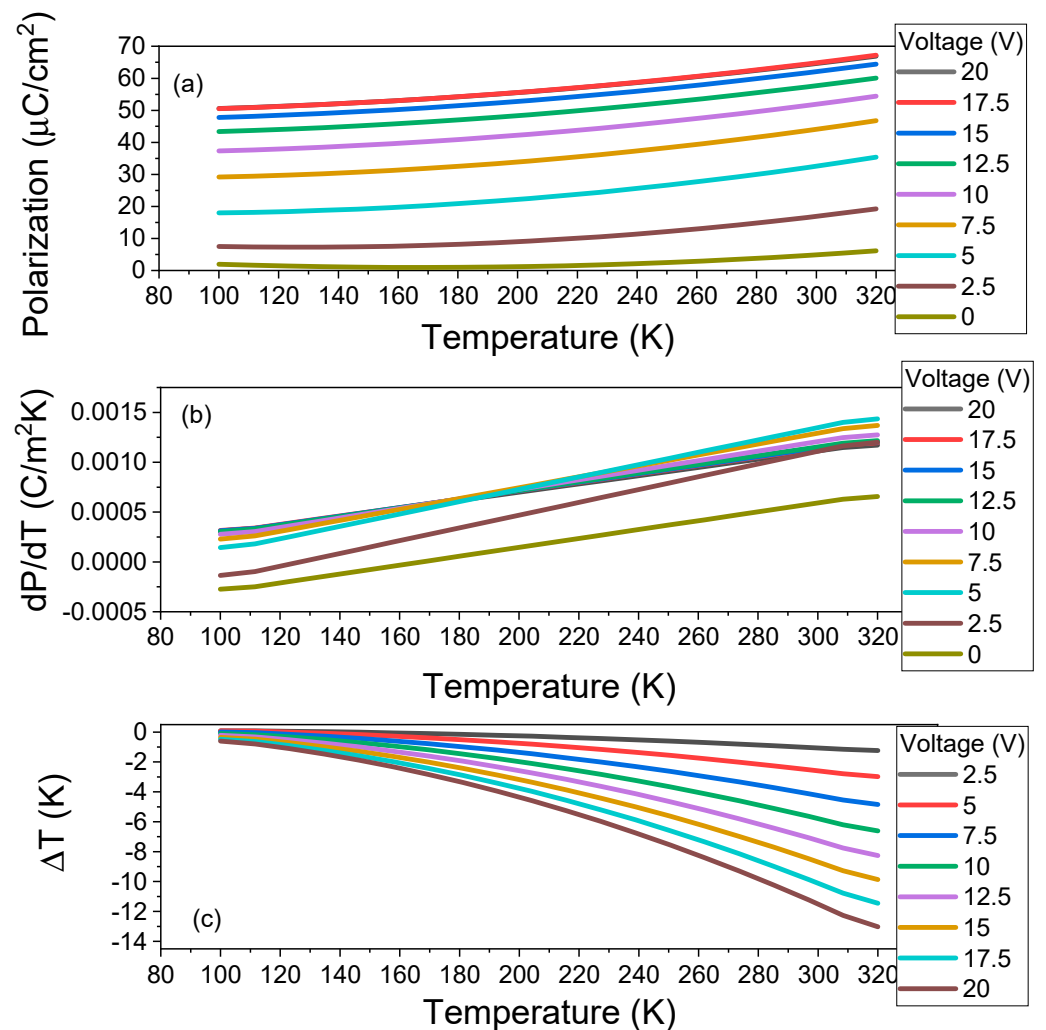
Figure 7. (**a**) The temperature dependence of polarization after switching for different voltages; (**b**) the indirectly evaluated pyroelectric coefficient as a function of temperature and different voltages; (**c**) the indirectly deduced adiabatic temperature variation as a function of temperature and voltages for epitaxial thin film Nb_2O_5/PZT/SRO/STO.

All the studied samples used the $\approx$200 nm thick epitaxial PZT layer as the common element, which was grown with similar conditions for all cases. The TEM investigation presented in the Supplementary Materials showed that there were no significant differences between the quality of the PZT layer for all five samples. The XRD performed at different temperatures showed no structural changes, which could be attributed to a phase transition or modification in the domain configurations. Thus, the only differences appeared from the different electrostatic conditions in the samples, which appeared to not only have a strong influence on the switching dynamic but also influence the variation in polarization with temperature. An assumption can be made that the interface formed with the electrodes, the polarization compensation phenomena, and the internal fields or defect dipoles induced by alternating layers with different electrical properties plays a crucial role in the way polarization reacts to temperature variations, which influences the pyroelectric and electrocaloric effects.

The structures fabricated with STON layers were analyzed for larger series resistances, and high switching times and large apparent coercive voltages at high frequencies were obtained. The voltage increase was distributed on the high resistive elements to generate increased charge currents to compensate for the polarization. A temperature increase led to

a faster polarization compensation by increasing the conductivity of the STON layer, which is related to a decrease in the coercive voltage but without any modification in polarization.

In ferroelectrics and dielectrics, ECE is related to changes in entropy corresponding to variations in polarization as the order parameter. When the temperature increases, the dipole-order decreases, polarization has a lower value, and the entropy increases. An applied voltage determines a higher order of dipoles, increasing the polarization and decreasing the entropy. During switching, a rearrangement of dipoles takes place, and thus the system passes through a disordered state and high entropy. During switching, a negative ECE may appear. This aspect is illustrated in Figure 8, where the Landau–Ginzbruch–Devonshire theory was used to obtain the polarization–voltage hysteresis curves for three different temperatures.
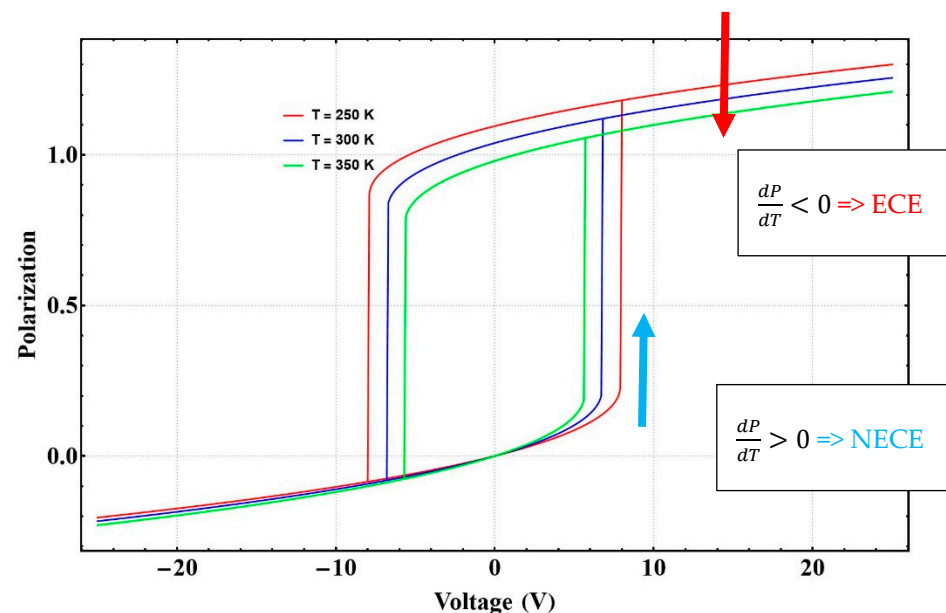

Figure 8. The theoretical polarization–voltage loops at different temperatures, deduced with classical thermodynamic treatment.

All our examples exhibited similar variations in polarization with the temperature near switching, but compared with the classical perspective, immediately after switching, a different variation in polarization with temperature may be possible, giving rise to either a normal or abnormal ECE.

Samples with relatively high internal fields, such as a simple PZT layer or BST/BST and Nb_2O_5/PZT, exhibited an abnormal negative ECE for the totally reversed state. For the multilayer situation, the evaluation was performed only on the positive voltage, since the polarization was almost totally back-switched when the voltage dropped to zero or had small negative values. For these cases, the internal electric field can be written as $E_{int} = \frac{-P*A}{C_s}$, where P is polarization, A is the area of the electrode, and C_S is the series capacitance of the insulator layer. After switching, the direction of the internal field opposes the polarization direction and generates a destabilization of the state order, resulting in an increase in entropy. Increasing the temperature conduction may increase the insulator layer, decreasing the depolarization effect of the series capacitor. Thus, a decrease in the internal electric field could justify an increased ferroelectric polar order, leading to a decrease in entropy and a negative ECE.

A similar mechanism may occur in a simple FE layer if we consider the formation of a Schottky barrier at the electrode interfaces. Depending on the voltage polarity, one of these barriers is depleted and could play the role of a series capacitance. Increasing the temperature, more charges are generated, leading to a decreasing disorder effect. A similar explanation still stands for the scenario of the dead-layer formation at the interface of the

FE thin films. The dead layer is considered to have zero polarization and thus could act as a series insulator thin film, with a very high associated series capacitance. Thus, the internal field was much smaller, compared with that of the multilayer case.

The abnormal negative ECE $\Delta T = -10.8$ K was also obtained in $Hf_xZr_{1-x}O_2$, which can be explained by the presence of different phases, with ferroelectric or non-ferroelectric order [39]. In a similar way, for a critical ratio between ferroelectric and non-ferroelectric depending on composition, a negative ECE could appear. Other examples of abnormal negative ECE are found in PZT-based multilayered thin films or in structures where ferroelectric material is mixed with a non-FE phase [16,40,41]. Additionally, the giant negative ECE is obtained in PZT/CFO multilayer structures [26], with up to $\Delta T = -52$ K. In all these examples, we can assume that the depolarization fields are key for abnormal polarization variation with temperature.

4. Conclusions

In this paper, the temperature dependence of ferroelectric polarization for different epitaxial thin film structures was investigated. An abnormal polarization increase at higher temperatures was revealed in simple PZT 20/80 thin film capacitor structures around room temperature, which could be attributed to a negative electrocaloric effect with a large adiabatic temperature change. Two different temperature variation behaviors of polarization were revealed in multilayered systems. When a resistive-like layer such as STON was deposited in contact with the FE layer, the polarization did not present a clear variation around room temperature. Otherwise, when an insulator layer such as BST or Nb_2O_5 came in contact with the FE layer, a similar negative electrocaloric effect was found. These results show that the internal field or defects determined by electrostatic conditions could induce large variations in polarization with the temperature for PZT-based epitaxial thin film structures around RT even if the transition temperature was much higher. Controlling the electrostatic conditions in FE heterostructures can overcome the classical and theoretical limitations predicting that, at temperatures lower than the transition temperature, the ECE is small, and the induced adiabatic temperature variation is insignificant, which represents a challenge in designing EC heat pumps. Moreover, we showed that, in this system, it is possible to obtain a negative ECE for the switching regime but, more importantly, also for voltages higher than the coercive voltage. This was another limitation for the potential applications of negative ECE during switching because, in classical results, after decreasing the system temperature during the disordered state of switching, usually follows a temperature increase due to the induced ordering by large applied fields.

This study also demonstrates the importance of the non-FE elements in the variation in polarization with temperature and can offer a better understanding of the mechanisms of positive or negative ECE. There are many examples in the literature of experimental ECE or negative ECE in relaxor, ferroelectric, and antiferroelectric materials [14,15,42,43] but also examples where experimentally no EC or abnormal EC effects appear in different materials even if theoretically they are EC materials [44].

Supplementary Materials: The following supporting information can be downloaded at: https://www.mdpi.com/article/10.3390/electronicmat3040028/s1, Figure S1. (a) The remnant hysteresis for 250 K, 300 K, and 350 K for PZT/SRO/STO; (b) The dependence of the indirect evaluated pyroelectric coefficient as a function of voltage for PZT/SRO/STO. Figure S2. The hysteresis measurements at different temperatures between 100 K and 300 K for polycrystalline sol–gel-deposited PZT/SRO/STO. Figure S3. (a) TEM image at low magnification (200 k) of the STON/PZT/SRO/STO heterostructure (insert: SAED image); (b) TEM image at low magnification (200 k) of the BST/PZT/SRO/STO heterostructure (insert: SAED image); (c) TEM image at low magnification (200 k) of the PZT/SRO/STO heterostructure (insert: SAED image).

References

1. Jia, Y.; Ju, Y.S. A Solid-State Refrigerator Based on the Electrocaloric Effect. *Appl. Phys. Lett.* **2012**, *100*, 242901. [CrossRef]
2. Ju, Y.S. Solid-State Refrigeration Based on the Electrocaloric Effect for Electronics Cooling. *J. Electron. Packag.* **2010**, *132*, 041004. [CrossRef]
3. Mischenko, A.S.; Zhang, Q.; Scott, J.F.; Whatmore, R.W.; Mathur, N.D. Giant Electrocaloric Effect in Thin-Film $PbZr_{0.95}Ti_{0.05}O_3$. *Science* **2006**, *311*, 1270–1271. [CrossRef]
4. Correia, T.; Zhang, Q. Electrocaloric Effect: An Introduction. In *Electrocaloric Materials: New Generation of Coolers*; Correia, T., Zhang, Q., Eds.; Engineering Materials; Springer: Berlin/Heidelberg, Germany, 2014; pp. 1–15. ISBN 978-3-642-40264-7.
5. Wiseman, G.G.; Kuebler, J.K. Electrocaloric Effect in Ferroelectric Rochelle Salt. *Phys. Rev.* **1963**, *131*, 2023–2027. [CrossRef]
6. Kutnjak, Z.; Rožič, B.; Pirc, R. Electrocaloric Effect: Theory, Measurements, and Applications. In *Wiley Encyclopedia of Electrical and Electronics Engineering*; John Wiley & Sons, Inc.: Hoboken, NJ, USA, 2015; pp. 1–19. ISBN 978-0-471-34608-1.
7. Peng, B.; Fan, H.; Zhang, Q. A Giant Electrocaloric Effect in Nanoscale Antiferroelectric and Ferroelectric Phases Coexisting in a Relaxor Pb0.8Ba0.2ZrO3 Thin Film at Room Temperature. *Adv. Funct. Mater.* **2013**, *23*, 2987–2992. [CrossRef]
8. Kutnjak, Z.; Rožič, B. Indirect and Direct Measurements of the Electrocaloric Effect. In *Electrocaloric Materials: New Generation of Coolers*; Engineering Materials; Correia, T., Zhang, Q., Eds.; Springer: Berlin/Heidelberg, Germany, 2014; pp. 147–182. ISBN 978-3-642-40264-7.
9. Liu, Y.; Scott, J.F.; Dkhil, B. Direct and Indirect Measurements on Electrocaloric Effect: Recent Developments and Perspectives. *Appl. Phys. Rev.* **2016**, *3*, 031102. [CrossRef]
10. Moya, X.; Kar-Narayan, S.; Mathur, N.D. Caloric Materials near Ferroic Phase Transitions. *Nat. Mater.* **2014**, *13*, 439–450. [CrossRef]
11. Marathe, M.; Grünebohm, A.; Nishimatsu, T.; Entel, P.; Ederer, C. First-Principles-Based Calculation of the Electrocaloric Effect in $BaTiO_3$: A Comparison of Direct and Indirect Methods. *Phys. Rev. B* **2016**, *93*, 054110. [CrossRef]
12. Takeuchi, I.; Sandeman, K. Solid-State Cooling with Caloric Materials. *Phys. Today* **2015**, *68*, 48–54. [CrossRef]
13. Fähler, S.; Rößler, U.K.; Kastner, O.; Eckert, J.; Eggeler, G.; Emmerich, H.; Entel, P.; Müller, S.; Quandt, E.; Albe, K. Caloric Effects in Ferroic Materials: New Concepts for Cooling. *Adv. Eng. Mater.* **2012**, *14*, 10–19. [CrossRef]
14. Geng, W.; Liu, Y.; Meng, X.; Bellaiche, L.; Scott, J.F.; Dkhil, B.; Jiang, A. Giant Negative Electrocaloric Effect in Antiferroelectric La-Doped Pb(ZrTi)O_3 Thin Films Near Room Temperature. *Adv. Mater.* **2015**, *27*, 3165–3169. [CrossRef] [PubMed]
15. Pirc, R.; Rožič, B.; Koruza, J.; Malič, B.; Kutnjak, Z. Negative Electrocaloric Effect in Antiferroelectric PbZrO3. *Eur. Lett.* **2014**, *107*, 17002. [CrossRef]
16. Zhang, T.; Li, W.; Hou, Y.; Yu, Y.; Cao, W.; Feng, Y.; Fei, W. Positive/Negative Electrocaloric Effect Induced by Defect Dipoles in PZT Ferroelectric Bilayer Thin Films. *RSC Adv.* **2016**, *6*, 71934–71939. [CrossRef]
17. Thacher, P.D. Electrocaloric Effects in Some Ferroelectric and Antiferroelectric Pb(Zr, Ti)O_3 Compounds. *J. Appl. Phys.* **1968**, *39*, 1996–2002. [CrossRef]
18. Wang, J.; Yang, T.; Wei, K.; Yao, X. Temperature–Electric Field Hysteresis Loop of Electrocaloric Effect in Ferroelectricity—Direct Measurement and Analysis of Electrocaloric Effect. I. *Appl. Phys. Lett.* **2013**, *102*, 152907. [CrossRef]
19. Wu, H.H.; Cohen, R.E. Polarization Rotation and the Electrocaloric Effect in Barium Titanate. *J. Phys. Condens. Matter* **2017**, *29*, 485704. [CrossRef] [PubMed]
20. Li, B.; Wang, J.B.; Zhong, X.L.; Wang, F.; Zeng, Y.K.; Zhou, Y.C. The Coexistence of the Negative and Positive Electrocaloric Effect in Ferroelectric Thin Films for Solid-State Refrigeration. *Eur. Lett.* **2013**, *102*, 47004. [CrossRef]
21. Marathe, M.; Renggli, D.; Sanlialp, M.; Karabasov, M.O.; Shvartsman, V.V.; Lupascu, D.C.; Grünebohm, A.; Ederer, C. Electrocaloric Effect in $BaTiO_3$ at All Three Ferroelectric Transitions: Anisotropy and Inverse Caloric Effects. *Phys. Rev. B* **2017**, *96*, 014102. [CrossRef]

22. Wu, H.H.; Cohen, R.E. Electric-Field-Induced Phase Transition and Electrocaloric Effect in PMN-PT. *Phys. Rev. B* **2017**, *96*, 054116. [CrossRef]

23. Li, B.; Wang, J.B.; Zhong, X.L.; Wang, F.; Zhou, Y.C. Room Temperature Electrocaloric Effect on PbZr$_{0.8}$Ti$_{0.2}$O3 Thin Film. *J. Appl. Phys.* **2010**, *107*, 014109. [CrossRef]

24. Akcay, G.; Alpay, S.P.; Mantese, J.V.; Rossetti, G.A., Jr. Magnitude of the Intrinsic Electrocaloric Effect in Ferroelectric Perovskite Thin Films at High Electric Fields. *Appl. Phys. Lett.* **2007**, *90*, 252909. [CrossRef]

25. Zuo, Z.; Chen, B.; Wang, B.; Yang, H.; Zhan, Q.; Liu, Y.; Wang, J.; Li, R.-W. Strain Assisted Electrocaloric Effect in PbZr$_{0.95}$Ti$_{0.05}$O$_3$ Films on 0.7Pb(Mg$_{1/3}$Nb$_{2/3}$)O$_3$-0.3PbTiO$_3$ Substrate. *Sci. Rep.* **2015**, *5*, 16164. [CrossRef] [PubMed]

26. Vats, G.; Kumar, A.; Ortega, N.; Bowen, C.R.; Katiyar, R.S. Giant Pyroelectric Energy Harvesting and a Negative Electrocaloric Effect in Multilayered Nanostructures. *Energy Environ. Sci.* **2016**, *9*, 1335–1345. [CrossRef]

27. Zhang, T.; Li, W.; Yu, Y.; Wang, M.; He, J.; Fei, W. Giant Electrocaloric Effect in Compositionally Graded PZT Multilayer Thin Films. *J. Alloys Compd.* **2018**, *731*, 489–495. [CrossRef]

28. Gariglio, S.; Stucki, N.; Triscone, J.-M.; Triscone, G. Strain Relaxation and Critical Temperature in Epitaxial Ferroelectric Pb(Zr$_{0.20}$Ti$_{0.80}$)O$_3$ Thin Films. *Appl. Phys. Lett.* **2007**, *90*, 202905. [CrossRef]

29. Pintilie, L.; Ghica, C.; Teodorescu, C.M.; Pintilie, I.; Chirila, C.; Pasuk, I.; Trupina, L.; Hrib, L.; Boni, A.G.; Georgiana Apostol, N.; et al. Polarization Induced Self-Doping in Epitaxial Pb(Zr$_{0.20}$Ti$_{0.80}$)O$_3$ Thin Films. *Sci. Rep.* **2015**, *5*, 14974. [CrossRef]

30. Chirila, C.; Boni, G.A.; Filip, L.D.; Husanu, M.; Neatu, S.; Istrate, C.M.; Le Rhun, G.; Vilquin, B.; Trupina, L.; Pasuk, I.; et al. Effect of Strain and Stoichiometry on the Ferroelectric and Pyroelectric Properties of the Epitaxial Pb(Zr$_{0.2}$Ti$_{0.80}$)O$_3$ Films Deposited on Si Wafers. *Mater. Sci. Eng. B Solid State Mater. Adv. Technol.* **2021**, *266*, 115042. [CrossRef]

31. Correia, T.M.; Young, J.S.; Whatmore, R.W.; Scott, J.F.; Mathur, N.D.; Zhang, Q. Investigation of the Electrocaloric Effect in a PbMg$_{2/3}$Nb$_{1/3}$O$_3$-PbTiO$_3$ Relaxor Thin Film. *Appl. Phys. Lett.* **2009**, *95*, 182904. [CrossRef]

32. Lu, S.G.; Rožič, B.; Zhang, Q.M.; Kutnjak, Z.; Li, X.; Furman, E.; Gorny, L.J.; Lin, M.; Malič, B.; Kosec, M.; et al. Organic and Inorganic Relaxor Ferroelectrics with Giant Electrocaloric Effect. *Appl. Phys. Lett.* **2010**, *97*, 162904. [CrossRef]

33. Niu, Z.-H.; Jiang, Y.-P.; Tang, X.-G.; Liu, Q.-X.; Li, W.-H.; Lin, X.-W.; Lu, S.-G. Giant Negative Electrocaloric Effect in B-Site Non-Stoichiometric (Pb$_{0.97}$La$_{0.02}$)(Zr$_{0.95}$Ti−0.05)1+yO$_3$ Anti-Ferroelectric Ceramics. *Mater. Res. Lett.* **2018**, *6*, 384–389. [CrossRef]

34. Cheng, X.; Weyland, F.; Novak, N.; Li, Y. Indirect Electrocaloric Evaluation: Influence of Polarization Hysteresis Measurement Frequency. *Phys. Status Solidi (A)* **2019**, *216*, 1900684. [CrossRef]

35. Chen, X.; Li, S.; Jian, X.; Hambal, Y.; Lu, S.-G.; Shvartsman, V.V.; Lupascu, D.C.; Zhang, Q.M. Maxwell Relation, Giant (Negative) Electrocaloric Effect, and Polarization Hysteresis. *Appl. Phys. Lett.* **2021**, *118*, 122904. [CrossRef]

36. Boni, G.A.; Chirila, C.F.; Stancu, V.; Amarande, L.; Pasuk, I.; Trupina, L.; Istrate, C.M.; Radu, C.; Tomulescu, A.; Neatu, S.; et al. Accidental Impurities in Epitaxial Pb(Zr$_{0.2}$Ti$_{0.8}$)O$_3$ Thin Films Grown by Pulsed Laser Deposition and Their Impact on the Macroscopic Electric Properties. *Nanomaterials* **2021**, *11*, 1177. [CrossRef] [PubMed]

37. Catalan, G.; Vlooswijk, A.H.G.; Janssens, A.; Rispens, G.; Redfern, S.; Rijnders, G.; Blank, D.H.A.; Noheda, B. X-ray Diffraction of Ferroelectric Nanodomains in Pbtio3 Thin Films. *Integr. Ferroelectr.* **2007**, *92*, 18–29. [CrossRef]

38. Negative Capacitance and Switching Dynamics Control Via Non-Ferroelectric Elements | ACS Applied Energy Materials. Available online: https://pubs.acs.org/doi/full/10.1021/acsaem.1c03890 (accessed on 21 July 2022).

39. Park, M.H.; Kim, H.J.; Kim, Y.J.; Moon, T.; Kim, K.D.; Lee, Y.H.; Hyun, S.D.; Hwang, C.S. Giant Negative Electrocaloric Effects of Hf$_{0.5}$Zr$_{0.5}$O$_2$ Thin Films. *Adv. Mater.* **2016**, *28*, 7956–7961. [CrossRef]

40. Bai, Y.; Zheng, G.-P.; Shi, S.-Q. Abnormal Electrocaloric Effect of Na$_{0.5}$Bi$_{0.5}$TiO$_3$–BaTiO$_3$ Lead-Free Ferroelectric Ceramics above Room Temperature. *Mater. Res. Bull.* **2011**, *46*, 1866–1869. [CrossRef]

41. Kaur, S.; Arora, M.; Kumar, S.; Malhi, P.S.; Singh, M.; Singh, A. Abnormal Electrocaloric Effect near Ambient Temperature in MgO Modified NBT-KBT. *Mater. Today Commun.* **2022**, *30*, 103028. [CrossRef]

42. Le Goupil, F.L.; Berenov, A.; Axelsson, A.-K.; Valant, M.; Alford, N.M. Direct and Indirect Electrocaloric Measurements on <001>-PbMg$_{1/3}$Nb$_{2/3}$O$_3$-30PbTiO$_3$ Single Crystals. *J. Appl. Phys.* **2012**, *111*, 124109. [CrossRef]

43. Peräntie, J.; Hagberg, J.; Uusimäki, A.; Jantunen, H. Electric-Field-Induced Dielectric and Temperature Changes in a ⟨011⟩-Oriented Pb (Mg$_{1/3}$Nb$_{2/3}$) O$_3$-PbTiO$_3$ Single Crystal. *Phys. Rev. B* **2010**, *82*, 134119. [CrossRef]

44. Rožič, B.; Kosec, M.; Uršič, H.; Holc, J.; Malič, B.; Zhang, Q.M.; Blinc, R.; Pirc, R.; Kutnjak, Z. Influence of the Critical Point on the Electrocaloric Response of Relaxor Ferroelectrics. *J. Appl. Phys.* **2011**, *110*, 064118. [CrossRef]